Branching Fraction Measurements of $B^+ \to \rho^+\gamma$, $B^0 \to \rho^0\gamma$, and $B^0 \to \omega\gamma$

B. Aubert,[1] M. Bona,[1] D. Boutigny,[1] Y. Karyotakis,[1] J. P. Lees,[1] V. Poireau,[1] X. Prudent,[1] V. Tisserand,[1] A. Zghiche,[1] E. Grauges,[2] A. Palano,[3] J. C. Chen,[4] N. D. Qi,[4] G. Rong,[4] P. Wang,[4] Y. S. Zhu,[4] G. Eigen,[5] I. Ofte,[5] B. Stugu,[5] G. S. Abrams,[6] M. Battaglia,[6] D. N. Brown,[6] J. Button-Shafer,[6] R. N. Cahn,[6] Y. Groysman,[6] R. G. Jacobsen,[6] J. A. Kadyk,[6] L. T. Kerth,[6] Yu. G. Kolomensky,[6] G. Kukartsev,[6] D. Lopes Pegna,[6] G. Lynch,[6] L. M. Mir,[6] T. J. Orimoto,[6] M. Pripstein,[6] N. A. Roe,[6] M. T. Ronan,[6,*] K. Tackmann,[6] W. A. Wenzel,[6] P. del Amo Sanchez,[7] M. Barrett,[7] T. J. Harrison,[7] A. J. Hart,[7] C. M. Hawkes,[7] A. T. Watson,[7] T. Held,[8] H. Koch,[8] B. Lewandowski,[8] M. Pelizaeus,[8] K. Peters,[8] T. Schroeder,[8] M. Steinke,[8] J. T. Boyd,[9] J. P. Burke,[9] W. N. Cottingham,[9] D. Walker,[9] D. J. Asgeirsson,[10] T. Cuhadar-Donszelmann,[10] B. G. Fulsom,[10] C. Hearty,[10] N. S. Knecht,[10] T. S. Mattison,[10] J. A. McKenna,[10] A. Khan,[11] P. Kyberd,[11] M. Saleem,[11] D. J. Sherwood,[11] L. Teodorescu,[11] V. E. Blinov,[12] A. D. Bukin,[12] V. P. Druzhinin,[12] V. B. Golubev,[12] A. P. Onuchin,[12] S. I. Serednyakov,[12] Yu. I. Skovpen,[12] E. P. Solodov,[12] K. Yu Todyshev,[12] M. Bondioli,[13] M. Bruinsma,[13] M. Chao,[13] S. Curry,[13] I. Eschrich,[13] D. Kirkby,[13] A. J. Lankford,[13] P. Lund,[13] M. Mandelkern,[13] E. C. Martin,[13] D. P. Stoker,[13] S. Abachi,[14] C. Buchanan,[14] S. D. Foulkes,[15] J. W. Gary,[15] F. Liu,[15] O. Long,[15] B. C. Shen,[15] L. Zhang,[15] E. J. Hill,[16] H. P. Paar,[16] S. Rahatlou,[16] V. Sharma,[16] J. W. Berryhill,[17] C. Campagnari,[17] A. Cunha,[17] B. Dahmes,[17] T. M. Hong,[17] D. Kovalskyi,[17] J. D. Richman,[17] T. W. Beck,[18] A. M. Eisner,[18] C. J. Flacco,[18] C. A. Heusch,[18] J. Kroseberg,[18] W. S. Lockman,[18] T. Schalk,[18] B. A. Schumm,[18] A. Seiden,[18] D. C. Williams,[18] M. G. Wilson,[18] L. O. Winstrom,[18] E. Chen,[19] C. H. Cheng,[19] A. Dvoretskii,[19] F. Fang,[19] D. G. Hitlin,[19] I. Narsky,[19] T. Piatenko,[19] F. C. Porter,[19] G. Mancinelli,[20] B. T. Meadows,[20] K. Mishra,[20] M. D. Sokoloff,[20] F. Blanc,[21] P. C. Bloom,[21] S. Chen,[21] W. T. Ford,[21] J. F. Hirschauer,[21] A. Kreisel,[21] M. Nagel,[21] U. Nauenberg,[21] A. Olivas,[21] J. G. Smith,[21] K. A. Ulmer,[21] S. R. Wagner,[21] J. Zhang,[21] A. Chen,[22] E. A. Eckhart,[22] A. Soffer,[22] W. H. Toki,[22] R. J. Wilson,[22] F. Winklmeier,[22] Q. Zeng,[22] D. D. Altenburg,[23] E. Feltresi,[23] A. Hauke,[23] H. Jasper,[23] J. Merkel,[23] A. Petzold,[23] B. Spaan,[23] K. Wacker,[23] T. Brandt,[24] V. Klose,[24] H. M. Lacker,[24] W. F. Mader,[24] R. Nogowski,[24] J. Schubert,[24] K. R. Schubert,[24] R. Schwierz,[24] J. E. Sundermann,[24] A. Volk,[24] D. Bernard,[25] G. R. Bonneaud,[25] E. Latour,[25] Ch. Thiebaux,[25] M. Verderi,[25] P. J. Clark,[26] W. Gradl,[26] F. Muheim,[26] S. Playfer,[26] A. I. Robertson,[26] Y. Xie,[26] M. Andreotti,[27] D. Bettoni,[27] C. Bozzi,[27] R. Calabrese,[27] G. Cibinetto,[27] E. Luppi,[27] M. Negrini,[27] A. Petrella,[27] L. Piemontese,[27] E. Prencipe,[27] F. Anulli,[28] R. Baldini-Ferroli,[28] A. Calcaterra,[28] R. de Sangro,[28] G. Finocchiaro,[28] S. Pacetti,[28] P. Patteri,[28] I. M. Peruzzi,[28,†] M. Piccolo,[28] M. Rama,[28] A. Zallo,[28] A. Buzzo,[29] R. Contri,[29] M. Lo Vetere,[29] M. M. Macri,[29] M. R. Monge,[29] S. Passaggio,[29] C. Patrignani,[29] E. Robutti,[29] A. Santroni,[29] S. Tosi,[29] K. S. Chaisanguanthum,[30] M. Morii,[30] J. Wu,[30] R. S. Dubitzky,[31] J. Marks,[31] S. Schenk,[31] U. Uwer,[31] D. J. Bard,[32] P. D. Dauncey,[32] R. L. Flack,[32] J. A. Nash,[32] M. B. Nikolich,[32] W. Panduro Vazquez,[32] P. K. Behera,[33] X. Chai,[33] M. J. Charles,[33] U. Mallik,[33] N. T. Meyer,[33] V. Ziegler,[33] J. Cochran,[34] H. B. Crawley,[34] L. Dong,[34] V. Eyges,[34] W. T. Meyer,[34] S. Prell,[34] E. I. Rosenberg,[34] A. E. Rubin,[34] A. V. Gritsan,[35] A. G. Denig,[36] M. Fritsch,[36] G. Schott,[36] N. Arnaud,[37] M. Davier,[37] G. Grosdidier,[37] A. Höcker,[37] V. Lepeltier,[37] F. Le Diberder,[37] A. M. Lutz,[37] S. Pruvot,[37] S. Rodier,[37] P. Roudeau,[37] M. H. Schune,[37] J. Serrano,[37] A. Stocchi,[37] W. F. Wang,[37] G. Wormser,[37] D. J. Lange,[38] D. M. Wright,[38] C. A. Chavez,[39] I. J. Forster,[39] J. R. Fry,[39] E. Gabathuler,[39] R. Gamet,[39] D. E. Hutchcroft,[39] D. J. Payne,[39] K. C. Schofield,[39] C. Touramanis,[39] A. J. Bevan,[40] K. A. George,[40] F. Di Lodovico,[40] W. Menges,[40] R. Sacco,[40] G. Cowan,[41] H. U. Flaecher,[41] D. A. Hopkins,[41] P. S. Jackson,[41] T. R. McMahon,[41] F. Salvatore,[41] A. C. Wren,[41] D. N. Brown,[42] C. L. Davis,[42] J. Allison,[43] N. R. Barlow,[43] R. J. Barlow,[43] Y. M. Chia,[43] C. L. Edgar,[43] G. D. Lafferty,[43] T. J. West,[43] J. I. Yi,[43] C. Chen,[44] W. D. Hulsbergen,[44] A. Jawahery,[44] C. K. Lae,[44] D. A. Roberts,[44] G. Simi,[44] G. Blaylock,[45] C. Dallapiccola,[45] S. S. Hertzbach,[45] X. Li,[45] T. B. Moore,[45] E. Salvati,[45] S. Saremi,[45] R. Cowan,[46] K. Koeneke,[46] M. I. Lang,[46] G. Sciolla,[46] S. J. Sekula,[46] M. Spitznagel,[46] F. Taylor,[46] R. K. Yamamoto,[46] M. Yi,[46] H. Kim,[47] S. E. Mclachlin,[47] P. M. Patel,[47] S. H. Robertson,[47] A. Lazzaro,[48] V. Lombardo,[48] F. Palombo,[48] J. M. Bauer,[49] L. Cremaldi,[49] V. Eschenburg,[49] R. Godang,[49] R. Kroeger,[49] D. A. Sanders,[49] D. J. Summers,[49] H. W. Zhao,[49] S. Brunet,[50] D. Côté,[50] M. Simard,[50] P. Taras,[50] F. B. Viaud,[50] H. Nicholson,[51] N. Cavallo,[52,‡] G. De Nardo,[52] F. Fabozzi,[52,‡] C. Gatto,[52] L. Lista,[52] D. Monorchio,[52] P. Paolucci,[52] D. Piccolo,[52] C. Sciacca,[52] M. A. Baak,[53] G. Raven,[53] H. L. Snoek,[53] C. P. Jessop,[54] J. M. LoSecco,[54] G. Benelli,[55] L. A. Corwin,[55] K. K. Gan,[55] K. Honscheid,[55] D. Hufnagel,[55] H. Kagan,[55] R. Kass,[55] J. P. Morris,[55] A. M. Rahimi,[55] J. J. Regensburger,[55] R. Ter-Antonyan,[55] Q. K. Wong,[55] N. L. Blount,[56] J. Brau,[56] R. Frey,[56] O. Igonkina,[56] J. A. Kolb,[56] M. Lu,[56] C. T. Potter,[56] R. Rahmat,[56] N. B. Sinev,[56] D. Strom,[56] J. Strube,[56] E. Torrence,[56] A. Gaz,[57] M. Margoni,[57] M. Morandin,[57] A. Pompili,[57] M. Posocco,[57] M. Rotondo,[57] F. Simonetto,[57] R. Stroili,[57] C. Voci,[57] E. Ben-Haim,[58]

H. Briand,[58] J. Chauveau,[58] P. David,[58] L. Del Buono,[58] Ch. de la Vaissière,[58] O. Hamon,[58] B. L. Hartfiel,[58] Ph. Leruste,[58] J. Malclès,[58] J. Ocariz,[58] L. Gladney,[59] M. Biasini,[60] R. Covarelli,[60] C. Angelini,[61] G. Batignani,[61] S. Bettarini,[61] G. Calderini,[61] M. Carpinelli,[61] R. Cenci,[61] F. Forti,[61] M. A. Giorgi,[61] A. Lusiani,[61] G. Marchiori,[61] M. A. Mazur,[61] M. Morganti,[61] N. Neri,[61] E. Paoloni,[61] G. Rizzo,[61] J. J. Walsh,[61] M. Haire,[62] J. Biesiada,[63] P. Elmer,[63] Y. P. Lau,[63] C. Lu,[63] J. Olsen,[63] A. J. S. Smith,[63] A. V. Telnov,[63] F. Bellini,[64] G. Cavoto,[64] A. D'Orazio,[64] D. del Re,[64] E. Di Marco,[64] R. Faccini,[64] F. Ferrarotto,[64] F. Ferroni,[64] M. Gaspero,[64] P. D. Jackson,[64] L. Li Gioi,[64] M. A. Mazzoni,[64] S. Morganti,[64] G. Piredda,[64] F. Polci,[64] C. Voena,[64] M. Ebert,[65] H. Schröder,[65] R. Waldi,[65] T. Adye,[66] G. Castelli,[66] B. Franek,[66] E. O. Olaiya,[66] S. Ricciardi,[66] W. Roethel,[66] F. F. Wilson,[66] R. Aleksan,[67] S. Emery,[67] M. Escalier,[67] A. Gaidot,[67] S. F. Ganzhur,[67] G. Hamel de Monchenault,[67] W. Kozanecki,[67] M. Legendre,[67] G. Vasseur,[67] Ch. Yèche,[67] M. Zito,[67] X. R. Chen,[68] H. Liu,[68] W. Park,[68] M. V. Purohit,[68] J. R. Wilson,[68] M. T. Allen,[69] D. Aston,[69] R. Bartoldus,[69] P. Bechtle,[69] N. Berger,[69] R. Claus,[69] J. P. Coleman,[69] M. R. Convery,[69] J. C. Dingfelder,[69] J. Dorfan,[69] G. P. Dubois-Felsmann,[69] D. Dujmic,[69] W. Dunwoodie,[69] R. C. Field,[69] T. Glanzman,[69] S. J. Gowdy,[69] M. T. Graham,[69] P. Grenier,[69] V. Halyo,[69] C. Hast,[69] T. Hryn'ova,[69] W. R. Innes,[69] M. H. Kelsey,[69] P. Kim,[69] D. W. G. S. Leith,[69] S. Li,[69] S. Luitz,[69] V. Luth,[69] H. L. Lynch,[69] D. B. MacFarlane,[69] H. Marsiske,[69] R. Messner,[69] D. R. Muller,[69] C. P. O'Grady,[69] V. E. Ozcan,[69] A. Perazzo,[69] M. Perl,[69] T. Pulliam,[69] B. N. Ratcliff,[69] A. Roodman,[69] A. A. Salnikov,[69] R. H. Schindler,[69] J. Schwiening,[69] A. Snyder,[69] J. Stelzer,[69] D. Su,[69] M. K. Sullivan,[69] K. Suzuki,[69] S. K. Swain,[69] J. M. Thompson,[69] J. Va'vra,[69] N. van Bakel,[69] A. P. Wagner,[69] M. Weaver,[69] W. J. Wisniewski,[69] M. Wittgen,[69] D. H. Wright,[69] H. W. Wulsin,[69] A. K. Yarritu,[69] K. Yi,[69] C. C. Young,[69] P. R. Burchat,[70] A. J. Edwards,[70] S. A. Majewski,[70] B. A. Petersen,[70] L. Wilden,[70] S. Ahmed,[71] M. S. Alam,[71] R. Bula,[71] J. A. Ernst,[71] V. Jain,[71] B. Pan,[71] M. A. Saeed,[71] F. R. Wappler,[71] S. B. Zain,[71] W. Bugg,[72] M. Krishnamurthy,[72] S. M. Spanier,[72] R. Eckmann,[73] J. L. Ritchie,[73] C. J. Schilling,[73] R. F. Schwitters,[73] J. M. Izen,[74] X. C. Lou,[74] S. Ye,[74] F. Bianchi,[75] F. Gallo,[75] D. Gamba,[75] M. Pelliccioni,[75] M. Bomben,[76] L. Bosisio,[76] C. Cartaro,[76] F. Cossutti,[76] G. Della Ricca,[76] L. Lanceri,[76] L. Vitale,[76] V. Azzolini,[77] N. Lopez-March,[77] F. Martinez-Vidal,[77] A. Oyanguren,[77] J. Albert,[78] Sw. Banerjee,[78] B. Bhuyan,[78] K. Hamano,[78] R. Kowalewski,[78] I. M. Nugent,[78] J. M. Roney,[78] R. J. Sobie,[78] J. J. Back,[79] P. F. Harrison,[79] T. E. Latham,[79] G. B. Mohanty,[79] M. Pappagallo,[79,§] H. R. Band,[80] X. Chen,[80] S. Dasu,[80] K. T. Flood,[80] J. J. Hollar,[80] P. E. Kutter,[80] B. Mellado,[80] Y. Pan,[80] M. Pierini,[80] R. Prepost,[80] S. L. Wu,[80] Z. Yu,[80] and H. Neal[81]

(*BABAR* Collaboration)

[1]*Laboratoire de Physique des Particules, IN2P3/CNRS et Université de Savoie, F-74941 Annecy-Le-Vieux, France*
[2]*Universitat de Barcelona, Facultat de Fisica, Departament ECM, E-08028 Barcelona, Spain*
[3]*Università di Bari, Dipartimento di Fisica and INFN, I-70126 Bari, Italy*
[4]*Institute of High Energy Physics, Beijing 100039, China*
[5]*University of Bergen, Institute of Physics, N-5007 Bergen, Norway*
[6]*Lawrence Berkeley National Laboratory and University of California, Berkeley, California 94720, USA*
[7]*University of Birmingham, Birmingham, B15 2TT, United Kingdom*
[8]*Ruhr Universität Bochum, Institut für Experimentalphysik 1, D-44780 Bochum, Germany*
[9]*University of Bristol, Bristol BS8 1TL, United Kingdom*
[10]*University of British Columbia, Vancouver, British Columbia, Canada V6T 1Z1*
[11]*Brunel University, Uxbridge, Middlesex UB8 3PH, United Kingdom*
[12]*Budker Institute of Nuclear Physics, Novosibirsk 630090, Russia*
[13]*University of California at Irvine, Irvine, California 92697, USA*
[14]*University of California at Los Angeles, Los Angeles, California 90024, USA*
[15]*University of California at Riverside, Riverside, California 92521, USA*
[16]*University of California at San Diego, La Jolla, California 92093, USA*
[17]*University of California at Santa Barbara, Santa Barbara, California 93106, USA*
[18]*University of California at Santa Cruz, Institute for Particle Physics, Santa Cruz, California 95064, USA*
[19]*California Institute of Technology, Pasadena, California 91125, USA*
[20]*University of Cincinnati, Cincinnati, Ohio 45221, USA*
[21]*University of Colorado, Boulder, Colorado 80309, USA*
[22]*Colorado State University, Fort Collins, Colorado 80523, USA*
[23]*Universität Dortmund, Institut für Physik, D-44221 Dortmund, Germany*
[24]*Technische Universität Dresden, Institut für Kern- und Teilchenphysik, D-01062 Dresden, Germany*
[25]*Laboratoire Leprince-Ringuet, CNRS/IN2P3, Ecole Polytechnique, F-91128 Palaiseau, France*
[26]*University of Edinburgh, Edinburgh EH9 3JZ, United Kingdom*

[27]*Università di Ferrara, Dipartimento di Fisica and INFN, I-44100 Ferrara, Italy*
[28]*Laboratori Nazionali di Frascati dell'INFN, I-00044 Frascati, Italy*
[29]*Università di Genova, Dipartimento di Fisica and INFN, I-16146 Genova, Italy*
[30]*Harvard University, Cambridge, Massachusetts 02138, USA*
[31]*Universität Heidelberg, Physikalisches Institut, Philosophenweg 12, D-69120 Heidelberg, Germany*
[32]*Imperial College London, London, SW7 2AZ, United Kingdom*
[33]*University of Iowa, Iowa City, Iowa 52242, USA*
[34]*Iowa State University, Ames, Iowa 50011-3160, USA*
[35]*Johns Hopkins University, Baltimore, Maryland 21218, USA*
[36]*Universität Karlsruhe, Institut für Experimentelle Kernphysik, D-76021 Karlsruhe, Germany*
[37]*Laboratoire de l'Accélérateur Linéaire, IN2P3/CNRS et Université Paris-Sud 11, Centre Scientifique d'Orsay, B. P. 34, F-91898 ORSAY Cedex, France*
[38]*Lawrence Livermore National Laboratory, Livermore, California 94550, USA*
[39]*University of Liverpool, Liverpool L69 7ZE, United Kingdom*
[40]*Queen Mary, University of London, E1 4NS, United Kingdom*
[41]*University of London, Royal Holloway and Bedford New College, Egham, Surrey TW20 0EX, United Kingdom*
[42]*University of Louisville, Louisville, Kentucky 40292, USA*
[43]*University of Manchester, Manchester M13 9PL, United Kingdom*
[44]*University of Maryland, College Park, Maryland 20742, USA*
[45]*University of Massachusetts, Amherst, Massachusetts 01003, USA*
[46]*Massachusetts Institute of Technology, Laboratory for Nuclear Science, Cambridge, Massachusetts 02139, USA*
[47]*McGill University, Montréal, Québec, Canada H3A 2T8*
[48]*Università di Milano, Dipartimento di Fisica and INFN, I-20133 Milano, Italy*
[49]*University of Mississippi, University, Mississippi 38677, USA*
[50]*Université de Montréal, Physique des Particules, Montréal, Québec, Canada H3C 3J7*
[51]*Mount Holyoke College, South Hadley, Massachusetts 01075, USA*
[52]*Università di Napoli Federico II, Dipartimento di Scienze Fisiche and INFN, I-80126, Napoli, Italy*
[53]*NIKHEF, National Institute for Nuclear Physics and High Energy Physics, NL-1009 DB Amsterdam, The Netherlands*
[54]*University of Notre Dame, Notre Dame, Indiana 46556, USA*
[55]*The Ohio State University, Columbus, Ohio 43210, USA*
[56]*University of Oregon, Eugene, Oregon 97403, USA*
[57]*Università di Padova, Dipartimento di Fisica and INFN, I-35131 Padova, Italy*
[58]*Laboratoire de Physique Nucléaire et de Hautes Energies, IN2P3/CNRS, Université Pierre et Marie Curie-Paris6, Université Denis Diderot-Paris7, F-75252 Paris, France*
[59]*University of Pennsylvania, Philadelphia, Pennsylvania 19104, USA*
[60]*Università di Perugia, Dipartimento di Fisica and INFN, I-06100 Perugia, Italy*
[61]*Università di Pisa, Dipartimento di Fisica, Scuola Normale Superiore and INFN, I-56127 Pisa, Italy*
[62]*Prairie View A&M University, Prairie View, Texas 77446, USA*
[63]*Princeton University, Princeton, New Jersey 08544, USA*
[64]*Università di Roma La Sapienza, Dipartimento di Fisica and INFN, I-00185 Roma, Italy*
[65]*Universität Rostock, D-18051 Rostock, Germany*
[66]*Rutherford Appleton Laboratory, Chilton, Didcot, Oxon, OX11 0QX, United Kingdom*
[67]*DSM/Dapnia, CEA/Saclay, F-91191 Gif-sur-Yvette, France*
[68]*University of South Carolina, Columbia, South Carolina 29208, USA*
[69]*Stanford Linear Accelerator Center, Stanford, California 94309, USA*
[70]*Stanford University, Stanford, California 94305-4060, USA*
[71]*State University of New York, Albany, New York 12222, USA*
[72]*University of Tennessee, Knoxville, Tennessee 37996, USA*
[73]*University of Texas at Austin, Austin, Texas 78712, USA*
[74]*University of Texas at Dallas, Richardson, Texas 75083, USA*
[75]*Università di Torino, Dipartimento di Fisica Sperimentale and INFN, I-10125 Torino, Italy*
[76]*Università di Trieste, Dipartimento di Fisica and INFN, I-34127 Trieste, Italy*
[77]*IFIC, Universitat de Valencia-CSIC, E-46071 Valencia, Spain*
[78]*University of Victoria, Victoria, British Columbia, Canada V8W 3P6*
[79]*Department of Physics, University of Warwick, Coventry CV4 7AL, United Kingdom*
[80]*University of Wisconsin, Madison, Wisconsin 53706, USA*
[81]*Yale University, New Haven, Connecticut 06511, USA*

(Received 11 December 2006; published 13 April 2007)

We present a study of the decays $B^+ \to \rho^+\gamma$, $B^0 \to \rho^0\gamma$, and $B^0 \to \omega\gamma$. The analysis is based on data containing 347×10^6 $B\bar{B}$ events recorded with the *BABAR* detector at the PEP-II asymmetric B factory.

We measure the branching fractions $\mathcal{B}(B^+ \to \rho^+\gamma) = (1.10^{+0.37}_{-0.33} \pm 0.09) \times 10^{-6}$ and $\mathcal{B}(B^0 \to \rho^0\gamma) = (0.79^{+0.22}_{-0.20} \pm 0.06) \times 10^{-6}$, and set a 90% C.L. upper limit $\mathcal{B}(B^0 \to \omega\gamma) < 0.78 \times 10^{-6}$. We also measure the isospin-averaged branching fraction $\mathcal{B}(B \to (\rho/\omega)\gamma) = (1.25^{+0.25}_{-0.24} \pm 0.09) \times 10^{-6}$, from which we determine $|V_{td}/V_{ts}| = 0.200^{+0.021}_{-0.020} \pm 0.015$, where the first uncertainty is experimental and the second is theoretical.

DOI: 10.1103/PhysRevLett.98.151802 PACS numbers: 13.20.He, 12.15.Hh, 14.40.Nd

In the standard model, the decays $B^+ \to \rho^+\gamma$, $B^0 \to \rho^0\gamma$, and $B^0 \to \omega\gamma$ [1] arise mainly from $b \to d\gamma$ penguin diagrams containing a virtual top quark in the loop. By relating the three individual decay rates by isospin symmetry and using the measured ratio between the charged and neutral B meson lifetimes τ_{B^+}/τ_{B^0}, an isospin-averaged branching fraction is defined: $\mathcal{B}(B \to (\rho/\omega)\gamma) \equiv \frac{1}{2}\{\mathcal{B}(B^+ \to \rho^+\gamma) + \frac{\tau_{B^+}}{\tau_{B^0}}[\mathcal{B}(B^0 \to \rho^0\gamma) + \mathcal{B}(B^0 \to \omega\gamma)]\}$. Recent calculations predict $\mathcal{B}(B \to (\rho/\omega)\gamma)$ to be in the range of $(0.9\text{–}1.8) \times 10^{-6}$ [2,3], where most of the uncertainty is due to the calculation of the form factor. These predictions could be modified by processes beyond the standard model [4].

While the exclusive decay rates have a large uncertainty due to nonperturbative long-distance QCD effects, some of this uncertainty cancels in the ratio of $\mathcal{B}(B \to (\rho/\omega)\gamma)$ to $B \to K^*\gamma$ branching fractions. Since the dominant diagram involves a virtual top quark, this ratio is related to the ratio of Cabibbo-Kobayashi-Maskawa matrix elements $|V_{td}/V_{ts}|$ [2,5] via

$$\frac{\mathcal{B}(B \to (\rho/\omega)\gamma)}{\mathcal{B}(B \to K^*\gamma)} = \left|\frac{V_{td}}{V_{ts}}\right|^2 \left(\frac{1 - m_\rho^2/M_B^2}{1 - m_{K^*}^2/M_B^2}\right)^3 \zeta^2[1 + \Delta R]. \quad (1)$$

The coefficient ζ is the ratio of the form factors for the decays $B \to \rho\gamma$ and $B \to K^*\gamma$ and ΔR accounts for different dynamics in the decay (e.g., annihilation diagrams can contribute to $B^+ \to \rho^+\gamma$). Physics beyond the standard model could affect these decays, creating inconsistencies between the measurement of $|V_{td}/V_{ts}|$ obtained from this analysis and that obtained from the ratio of B^0 and B_s^0 mixing frequencies [6].

Previous searches by *BABAR* [7] and CLEO [8] found no evidence for the decays $B \to \rho\gamma$ and $B \to \omega\gamma$. An observation of the decay $B^0 \to \rho^0\gamma$ was recently reported by the Belle Collaboration [9]. This Letter reports on a study of the decays $B^+ \to \rho^+\gamma$, $B^0 \to \rho^0\gamma$, and $B^0 \to \omega\gamma$ based on a data sample containing 347×10^6 $B\bar{B}$ events, corresponding to an integrated luminosity of 316 fb^{-1}, collected with the *BABAR* detector [10] at the PEP-II asymmetric-energy e^+e^- storage ring. These results supersede the previous *BABAR* measurements [7].

The decays $B \to \rho\gamma$ and $B \to \omega\gamma$ are reconstructed by combining a high-energy photon with a vector meson reconstructed in the decay modes $\rho^0 \to \pi^+\pi^-$ ($\mathcal{B} \sim 100\%$), $\rho^+ \to \pi^+\pi^0$ ($\mathcal{B} \sim 100\%$), and $\omega \to \pi^+\pi^-\pi^0$ ($\mathcal{B} = [89.1 \pm 0.7]\%$) [11].

The dominant source of background is continuum events ($e^+e^- \to q\bar{q}$, with $q = u, d, s, c$) that contain a high-energy photon from π^0 or η decays. Other backgrounds include photons from initial-state radiation (ISR) processes, decays of $B \to K^*\gamma$ ($K^* \to K\pi$), decays of $B \to (\rho/\omega)\pi^0$ or $B \to (\rho/\omega)\eta$ and combinatorial background from higher-multiplicity $b \to s\gamma$ decays. For each signal decay mode, selection requirements have been optimized for maximum statistical sensitivity with assumed signal branching fractions of 1.0×10^{-6} and 0.5×10^{-6} for the charged and neutral modes, respectively.

The photon from a signal B decay is identified as a well-isolated energy deposit in the electromagnetic calorimeter with energy $1.5 < E_\gamma^* < 3.5\text{GeV}$ in the center of mass (c.m.) frame. The energy deposit must not be associated with any charged track and must meet several other requirements designed to eliminate background from hadronic showers and charged particles [12]. In order to veto photons from π^0 and η decays, we associate each high-energy photon candidate γ with each of the other photons γ' in the event. We reject the candidates that are consistent with originating from π^0 or η decays based on a likelihood ratio constructed from the energy of the second photon γ' and the invariant mass of the pair $m_{\gamma\gamma'}$. We also combine the high-energy photon candidate with photon conversions to e^+e^- pairs, and reject the photon if the invariant mass is consistent with a π^0 or η.

Charged-pion candidates are selected from well-reconstructed tracks with a minimum momentum transverse to the beam direction of 100 MeV/c. A stringent $\pi^\pm$ selection algorithm [7] is applied to reduce background from charged kaons produced in $b \to s\gamma$ decays. The algorithm combines the information provided by the ring-imaging Cherenkov detector with the measurement of energy loss in the tracking system.

Photon candidates with energy greater than 50 MeV in the laboratory frame are combined into pairs to form π^0 candidates. For $B^0 \to \omega\gamma$ ($B^+ \to \rho^+\gamma$) decays, the invariant mass of the pair is required to satisfy $122 < m_{\gamma\gamma} < 150$ MeV/c^2 ($117 < m_{\gamma\gamma} < 148$ MeV/c^2). We also require that the cosine of the opening angle between the daughter photons in the laboratory frame be greater than 0.413 (0.789).

The identified pions are combined into vector meson candidates by requiring $633 < m_{\pi^+\pi^-} < 957$ MeV/c^2, $636 < m_{\pi^+\pi^0} < 932$ MeV/c^2, and $764 < m_{\pi^+\pi^-\pi^0} < 795$ MeV/c^2 for ρ^0, ρ^+, and ω, respectively. The charged-pion pairs must originate from a common vertex.

The separation along the beam axis between this vertex and the one obtained by combining the other charged particles in the event is required to be less than 4 mm and to be measured with a precision better than 0.4 mm.

The photon and ρ/ω candidates are combined to form the B meson candidates. We define $\Delta E \equiv E_B^* - E_{\rm beam}^*$, where E_B^* is the c.m. energy of the B meson candidate and $E_{\rm beam}^*$ is the c.m. beam energy. We also define the beam-energy-substituted mass $m_{\rm ES} \equiv \sqrt{E_{\rm beam}^{*2} - p_B^{*2}}$, where p_B^* is the c.m. momentum of the B candidate. Signal events are expected to have a ΔE distribution centered near zero with a resolution of about 50 MeV, and an $m_{\rm ES}$ distribution centered at the mass of the B meson, with a resolution of 3 MeV/c^2. We consider candidates in the ranges $-0.3 < \Delta E < 0.3$ GeV and $m_{\rm ES} > 5.22$ GeV/c^2, which include sidebands that allow the combinatorial background yields to be extracted from a fit to the data.

In signal events the vector meson is transversely polarized, while in background events from $B \to \rho(\pi^0/\eta)$ and $B \to \omega(\pi^0/\eta)$ it is longitudinally polarized. To reject this background, we calculate the vector meson helicity angle θ_H and require $|\cos\theta_H| < 0.75$. The helicity angle is defined as the angle between the B momentum vector and the π^- track calculated in the ρ rest frame in the case of a ρ meson, or the angle between the B momentum vector and the normal to the ω decay plane for an ω meson.

Contributions from continuum background processes are reduced by considering only events for which the ratio R_2 of second-to-zeroth Fox-Wolfram moments [13] calculated using the momenta of all charged and neutral particles in the event is less than 0.7. A neural network combining the variables described below further suppresses the continuum background. The quantity R_2', defined as R_2 in the frame recoiling against the photon momentum, is used to reject ISR events. To discriminate between the jetlike continuum background and the more spherically symmetric signal events, we compute the angle between the photon and the thrust axis of the rest of the event (ROE) in the c.m. frame. The ROE is defined by all charged tracks and neutral energy deposits in the calorimeter that are not used to reconstruct the B candidate. We also calculate the moments $L_i \equiv \sum_j p_j^* |\cos\theta_j^*|^i / \sum_j p_j^*$, where p_j^* and θ_j^* are the momentum and angle with respect to an axis, respectively, for each particle j in the ROE. We use L_1, L_2, and L_3 with respect to the thrust axis of the ROE, as well as with respect to the photon direction. In addition, we calculate the B meson production angle θ_B^* with respect to the beam axis in the c.m. frame. Differences in lepton and kaon production between background and B decays are exploited by using flavor-tagging variables [14]. The significance of the separation along the beam axis of the B meson candidate and ROE vertices is included as well. The purity of the selected sample is enhanced by a cut on the output of the neural network that retains 63%, 74%, and 71% of the signal events in the modes $B^+ \to \rho^+\gamma$, $B^0 \to \rho^0\gamma$, and $B^0 \to \omega\gamma$, respectively.

The expected average candidate multiplicity in the selected signal events is 1.01 for $B^0 \to \rho^0\gamma$ and 1.07 for both $B^+ \to \rho^+\gamma$ and $B^0 \to \omega\gamma$. In events with multiple candidates, the one with the reconstructed vector meson mass closest to the nominal mass is retained. This criteria was chosen because the mass of the vector meson was found to be uncorrelated with the variables used in the fit. Applying all the selection criteria described above, we find efficiencies [15] of 11.0% for $B^+ \to \rho^+\gamma$, 14.1% for $B^0 \to \rho^0\gamma$, and 7.9% for $B^0 \to \omega\gamma$.

The signal content of the data is determined by a multidimensional unbinned maximum likelihood fit, which is constructed individually for each of the three signal decay modes. All fits use ΔE, $m_{\rm ES}$, $\cos\theta_H$, and the neural network output N. In order to facilitate the parametrization of the probability density function (PDF) used in the fit, the transformation $\mathcal{NN} = \tanh^{-1}(c_1 N - c_2)$, in which the c_i are mode-dependent constants, is made. For decays $B^0 \to \omega\gamma$ ($\omega \to \pi^+\pi^-\pi^0$), the cosine of the angle between the π^+ and π^0 momenta in the $\pi^+\pi^-$ rest frame (Dalitz angle) is added as a fifth observable.

In the fit we consider several hypotheses for the origin of the events: signal, continuum background, $B \to K^*\gamma$ decays, and other B backgrounds. The likelihood function for a signal mode k ($= \rho^+\gamma$, $\rho^0\gamma$, $\omega\gamma$) is defined as

$$\mathcal{L}_k = \exp\Big(-\sum_{i=1}^{N_{\rm hyp}} n_i\Big)\Big[\prod_{j=1}^{N_k}\Big(\sum_{i=1}^{N_{\rm hyp}} n_i \mathcal{P}_i(\vec{x}_j;\vec{\alpha}_i)\Big)\Big], \quad (2)$$

where $N_{\rm hyp}$ is the number of event hypotheses, n_i is the yield of each hypothesis, and N_k is the number of candidate events observed in data. Since the correlations among the observables are found to be small in simulated event samples, we define the PDF $\mathcal{P}_i(\vec{x}_j;\vec{\alpha}_i)$ for the ith event hypothesis as the product of individual PDFs for each fit observable x_j given the set of parameters $\vec{\alpha}_i$.

Each PDF is determined from a one-dimensional fit to a dedicated sample of simulated events. The ΔE PDF is corrected for the observed difference between data and simulation by using samples of $B \to K^*\gamma$ decays. All continuum background parameters float freely in the fits, while the shapes of the signal and B background distributions are fixed according to the Monte Carlo simulation. The signal $m_{\rm ES}$ spectra are described by crystal ball functions [16], the angular distributions are modeled by polynomials, and the distributions of ΔE and $\mathcal{NN}$ are parametrized as $f(x) = \exp\Big(\frac{-(x-\mu)^2}{2\sigma_{L,R}^2 + \alpha_{L,R}(x-\mu)^2}\Big)$, where μ is the peak position of the distribution, $\sigma_{L,R}$ are the widths on the left and right of the peak, and $\alpha_{L,R}$ are a measure of the tails on the left and right of the peak, respectively. Various functional forms are used to describe the continuum and B background components.

We measure the signal yield $n_{\rm sig}$ by maximizing the likelihood function in Eq. (2). In the fit, the continuum background yield is allowed to float, as is the overall yield of the B background, with the exception of the $B^+ \to K^{*+}\gamma$ ($K^{*+} \to K^+\pi^0$) yield in the $B^+ \to \rho^+\gamma$ mode, which is fixed. The relative yields among the different B backgrounds are fixed to the values obtained using known branching fractions [11] and selection efficiencies determined from simulated events. Figure 1 shows the data points and the projections of the fit results for ΔE and $m_{\rm ES}$ separately for each decay mode. The signal yields are reported in Table I. The significance is computed as $\sqrt{2\Delta \log \mathcal{L}}$, where $\Delta \log \mathcal{L}$ is the log-likelihood difference between the best fit and the null-signal hypothesis.

Table II gives an overview of the contributions to the systematic uncertainties. These are associated with the signal reconstruction efficiency and the modeling of signal and $B\bar{B}$ background in the Monte Carlo simulation. The latter contributes to the uncertainties on the signal yields. The systematic error affecting the signal efficiency includes uncertainties on tracking, particle identification, γ and π^0 reconstruction, π^0/η veto, and the neural network selection. The uncertainties on the π^0/η veto and neural network selection are determined from a control sample of $B \to D\pi$ decays, with $D \to K\pi$ or $D \to K\pi\pi$. To estimate the uncertainty related to the modeling of the signal and B background in the Monte Carlo, we vary the parameters of the PDFs that are fixed in the fit within their errors. The uncertainty related to the choice of a specific functional form for the shape of the $\mathcal{NN}$ distribution is evaluated by using a binned PDF as an alternative description. All relative and absolute normalizations of B background components that are fixed in the fit are varied within their errors. For all these variations, the corresponding change in the fitted signal yield is taken as a systematic uncertainty.

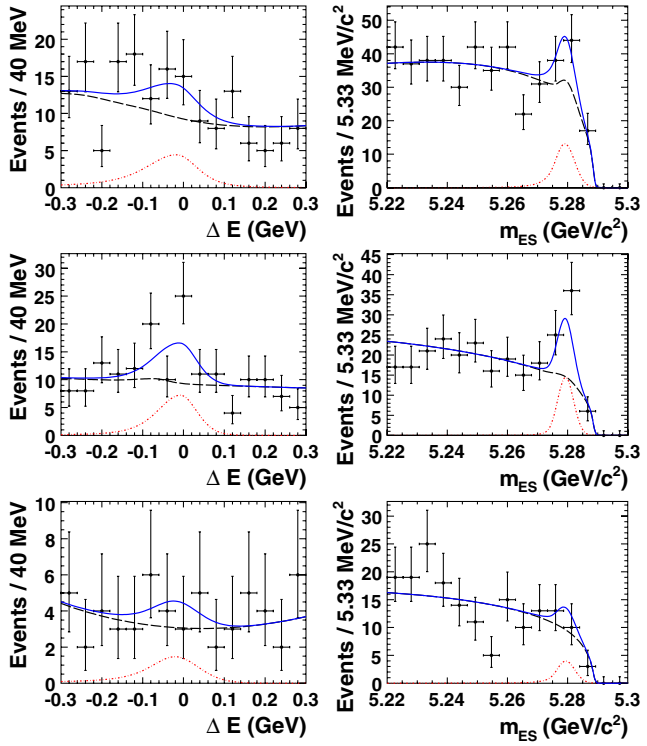

FIG. 1 (color online). ΔE and $m_{\rm ES}$ projections of the fits for the decay modes $B^+ \to \rho^+\gamma$ (top), $B^0 \to \rho^0\gamma$ (middle), and $B^0 \to \omega\gamma$ (bottom). In each plot, the signal fraction is enhanced by selections on the other fit variables. The points are data, the solid line is the total of all contributions, and the long-dashed (dash-dotted) line is background only (signal only).

The branching fractions are calculated from the measured signal yields assuming $\mathcal{B}(\Upsilon(4S) \to B^0\bar{B}^0) = \mathcal{B}(\Upsilon(4S) \to B^+B^-) = 0.5$. The results are listed in Table I. For $B^0 \to \omega\gamma$, we also compute the 90% confidence level (C.L.) upper limit $\mathcal{B}(B^0 \to \omega\gamma) < 0.78 \times 10^{-6}$ using a Bayesian technique. We determine the branching fraction upper limit $\mathcal{B}_l$ such that $\int_0^{\mathcal{B}_l} \mathcal{L}d\mathcal{B} / \int_0^{\infty} \mathcal{L}d\mathcal{B} = 0.90$, assuming a flat prior in the branching fraction and taking into account the systematic uncertainty.

We test the hypothesis of isospin symmetry by measuring the quantity $\Gamma(B^+ \to \rho^+\gamma)/[2\Gamma(B^0 \to \rho^0\gamma)] - 1 = -0.35 \pm 0.27$. The result is consistent with the theoretical expectation [2].

The isospin-averaged branching fraction is extracted from a simultaneous fit to the three decay modes:

$$\mathcal{B}(B \to (\rho/\omega)\gamma) = (1.25^{+0.25}_{-0.24} \pm 0.09) \times 10^{-6}. \quad (3)$$

In the fit we impose the isospin constraints on the widths of the decay modes: $\Gamma_{B\to\rho^+\gamma} = 2\Gamma_{B\to\rho^0\gamma} = 2\Gamma_{B\to\omega\gamma}$. Our measurements of the individual branching fractions are consistent with this hypothesis with a χ^2 of 1.8 for 2 degrees of freedom. The significance of the signal is 6.4σ, including systematic uncertainties. This result is consistent with the measurement from Belle [9]. If we exclude the $B^0 \to \omega\gamma$ mode from the simultaneous fit, we obtain $\mathcal{B}(B \to \rho\gamma) = (1.36^{+0.29}_{-0.27} \pm 0.10) \times 10^{-6}$. Using the world average value of $\mathcal{B}(B \to K^*\gamma)$ [11], we

TABLE I. The signal yield ($n_{\rm sig}$), significance (Σ) in standard deviations including systematic errors, efficiency (ϵ), and branching fraction ($\mathcal{B}$) for each mode. The errors on $n_{\rm sig}$ are statistical only, while for the branching fraction the first error is statistical and the second systematic.

Mode	$n_{\rm sig}$	Σ	$\epsilon(\%)$	$\mathcal{B}(10^{-6})$
$B^+ \to \rho^+\gamma$	$42.0^{+14.0}_{-12.7}$	3.8σ	11.0	$1.10^{+0.37}_{-0.33} \pm 0.09$
$B^0 \to \rho^0\gamma$	$38.7^{+10.6}_{-9.8}$	4.9σ	14.1	$0.79^{+0.22}_{-0.20} \pm 0.06$
$B^0 \to \omega\gamma$	$11.0^{+6.7}_{-5.6}$	2.2σ	7.9	$0.40^{+0.24}_{-0.20} \pm 0.05$
$B \to (\rho/\omega)\gamma$		6.4σ		$1.25^{+0.25}_{-0.24} \pm 0.09$
$B \to \rho\gamma$		6.0σ		$1.36^{+0.29}_{-0.27} \pm 0.10$

TABLE II. Fractional systematic errors (in %) of the measured branching fractions.

Source of error	$\rho^+\gamma$	$\rho^0\gamma$	$\omega\gamma$	$\rho\gamma$	$(\rho/\omega)\gamma$
Tracking efficiency	1.0	2.0	2.0	1.4	1.5
Particle identification	2.0	4.0	2.0	2.9	2.7
Photon selection	1.9	2.6	1.7	2.2	2.1
π^0 reconstruction	3.0	...	3.0	1.9	2.5
π^0 and η veto	2.8	2.8	2.8	2.8	2.8
$\mathcal{NN}$ efficiency	1.0	1.0	1.0	1.0	1.0
$\mathcal{NN}$ shape	0.4	0.3	2.3	0.4	0.7
Signal PDF shapes	4.8	3.3	2.4	3.1	2.6
B background PDFs	3.9	2.9	9.7	3.2	3.1
$B\bar{B}$ sample size	1.1	1.1	1.1	1.1	1.1
$\mathcal{B}(\omega \to \pi^+\pi^-\pi^0)$	...	...	0.8	...	0.1
Sum in quadrature	8.1	7.4	11.6	7.0	6.9

calculate $\mathcal{B}(B\to(\rho/\omega)\gamma)/\mathcal{B}(B\to K^*\gamma) = 0.030 \pm 0.006$. This result can be used to calculate the ratio $|V_{td}/V_{ts}|$ [2,17,18]. Following [17], we obtain

$$|V_{td}/V_{ts}| = 0.200^{+0.021}_{-0.020} \pm 0.015, \quad (4)$$

where the first error is experimental and the second is theoretical. This result is consistent with the measurement of this ratio from the study of B^0 and B_s^0 mixing [6].

In conclusion, we have measured the branching fractions of $\mathcal{B}(B^+ \to \rho^+\gamma) = (1.10^{+0.37}_{-0.33} \pm 0.09) \times 10^{-6}$ and $\mathcal{B}(B^0 \to \rho^0\gamma) = (0.79^{+0.22}_{-0.20} \pm 0.06) \times 10^{-6}$, and set a 90% C.L. upper limit on the $B^0 \to \omega\gamma$ branching fraction of $\mathcal{B}(B^0 \to \omega\gamma) < 0.78 \times 10^{-6}$. The isospin-averaged branching fraction $\mathcal{B}(B \to (\rho/\omega)\gamma) = (1.25^{+0.25}_{-0.24} \pm 0.09) \times 10^{-6}$ is the most precise measurement of this quantity to date. This measurement is used to extract $|V_{td}/V_{ts}| = 0.200^{+0.021}_{-0.020} \pm 0.015$.

We are grateful for the excellent luminosity and machine conditions provided by our PEP-II colleagues, and for the substantial dedicated effort from the computing organizations that support *BABAR*. The collaborating institutions wish to thank SLAC for its support and kind hospitality. This work is supported by DOE and NSF (U.S.), NSERC (Canada), IHEP (China), CEA and CNRS-IN2P3 (France), BMBF and DFG (Germany), INFN (Italy), FOM (The Netherlands), NFR (Norway), MIST (Russia), MEC (Spain), and PPARC (U.K.). Individuals have received support from the Marie Curie EIF (E.U.) and the A. P. Sloan Foundation.

*Deceased.
†Also with Università di Perugia, Dipartimento di Fisica, Perugia, Italy.
‡Also with Università della Basilicata, Potenza, Italy.
§Also with IPPP, Physics Department, Durham University, Durham DH1 3LE, United Kingdom.

[1] Charge conjugate modes are implied throughout.
[2] A. Ali, E. Lunghi, and A. Y. Parkhomenko, Phys. Lett. B **595**, 323 (2004).
[3] S. W. Bosch and G. Buchalla, Nucl. Phys. **B621**, 459 (2002).
[4] See, for example, S. Bertolini, F. Borzumati, and A. Masiero, Nucl. Phys. **B294**, 321 (1987); H. Baer and M. Brhlik, Phys. Rev. D **55**, 3201 (1997); J. Hewett and J. Wells, Phys. Rev. D **55**, 5549 (1997); M. Carena *et al.*, Phys. Lett. B **499**, 141 (2001).
[5] A. Ali and A. Y. Parkhomenko, Eur. Phys. J. C **23**, 89 (2002).
[6] A. Abulencia *et al.*, Phys. Rev. Lett. **97**, 242003 (2006).
[7] B. Aubert *et al.*, Phys. Rev. Lett. **94**, 011801 (2005).
[8] T. E. Coan *et al.*, Phys. Rev. Lett. **84**, 5283 (2000).
[9] D. Mohapatra *et al.*, Phys. Rev. Lett. **96**, 221601 (2006).
[10] B. Aubert *et al.*, Nucl. Instrum. Methods Phys. Res., Sect. A **479**, 1 (2002).
[11] W. M. Yao *et al.*, J. Phys. G **33**, 1 (2006).
[12] B. Aubert *et al.*, Phys. Rev. Lett. **88**, 101805 (2002).
[13] G. C. Fox and S. Wolfram, Nucl. Phys. **B149**, 413 (1979).
[14] B. Aubert *et al.*, Phys. Rev. Lett. **89**, 201802 (2002).
[15] The efficiency quoted for the ω mode includes the branching fraction for the decay $\omega \to \pi^+\pi^-\pi^0$.
[16] J. E. Gaiser *et al.*, Phys. Rev. D **34**, 711 (1986).
[17] P. Ball and R. Zwicky, J. High Energy Phys. 04 (2006) 046; P. Ball, G. Jones, and R. Zwicky, Phys. Rev. D **75**, 054004 (2007).
[18] S. W. Bosch and G. Buchalla, J. High Energy Phys. 01 (2005) 035.